Available online at www.sciencedirect.com
ScienceDirect
ELSEVIER
Composites Science and Technology 67 (2007) 1553–1560
COMPOSITES SCIENCE AND TECHNOLOGY
www.elsevier.com/locate/compscitech

A generalized self consistent model for effective elastic moduli of human dentine

Yanan Wang [a], Qing-Hua Qin [b,*]

[a] *Department of Mechanics, Tianjin University, Tianjin, 300072, China*
[b] *Department of Engineering, Australian National University, Canberra, Australia*

Received 20 April 2006; received in revised form 14 July 2006; accepted 17 July 2006
Available online 12 September 2006

Abstract

Closed-form expressions are presented for effective material properties of human dentine in this paper. The derivation is based a Generalized Self Consistent Method and the strain energy principle. The Generalized Self Consistent Model for cell model of fiber-reinforced composites is extended to the case of hollow cylinder model and the corresponding cell model is chosen to consist of a circular hollow cylinder filled with liquid or gas phase, which surrounded by a circular cylindrical shell of matrix phase. Each layer of cylindrical shell is here considered as a kind of composite consisting of collagen fibrils, with mineralized hydroxyapatite, loosely connected to their neighbours, and water (or gas in the case of dry dentine composite). Using the cell model, the effect of Poisson's ratio and volume fraction of intertubular dentine on effective mechanical constants is analyzed. Results obtained from the proposed model are compared with those from other models such as nano-indentation method.

Keywords: B. Human dentine; B. Generalized Self Consistent Method; B. Effective mechanical properties; B. Fiber-reinforced; B. Collagen

1. Introduction

Human dentine, the mineralized tissue forming the bulk of the tooth, lies between the enamel and the pulp chamber. It has a characteristic micro-structure consisting of a hydrated matrix of type I collagen that is reinforced with a nano-crystalline carbonated apatite. This matrix phase lies between nearly cylindrical tubules that run from the dentine–enamel junction to the pulp chamber [1]. Along with the development of dentistry medicine, people begin to realize that the effective elastic properties of dentine are of considerable importance for nearly all surgical procedures in preventive and restorative dentistry [2].

Recently, there has been considerable theoretical work directly toward fiber-reinforced composites and dentine like composites [3,4]. Christensen [3] developed a micromechanics model of solid cylindrical inclusions in a homogeneous matrix phase, which is very useful for that it permits the limiting case of full packing of the inclusion phase, with $c \to 1$, where c is the volume fraction of the inclusion phase. In contrast, most conventional composites in which only the matrix phase is spatially continuous and no porosity or liquid phase is involved, dentine is a porous interpenetrating phase composite that has several phases such as collagen fibrils, mineralized hydroxyapatite and water that are each interconnected in three dimensions and construct a topologically continuous network throughout the composite [4]. As mentioned above, dentine microstructure and properties are principal determinants of nearly all surgical procedures in preventive and restorative dentistry, the determination of the effective mechanical properties of dentine, a multi-phase composite, is of great interest for both its biomedical engineering applications and theoretical analysis. However there has been little previous theoretical work on this specific subject. Kinney et al. [1] studied the effect of tubule orientation on the elastic properties of dentine using a micro-mechanics model of

* Corresponding author. Tel.: +61 2 61258274; fax: +61 2 61250506.
E-mail address: qinghua.qin@anu.edu.au (Q.-H. Qin).

0266-3538/$ - see front matter
doi:10.1016/j.compscitech.2006.07.014

cylindrical inclusions in a homogeneous matrix phase [3]. Currey [4] examined experimentally the effect of porosity and mineral content on the Young's modulus of elasticity of compact bone. He indicated that there was a strong positive relationship between Young's modulus and both calcium content and volume fraction and a power law model fits the data better than a linear model. Jones and Boyde [5] presented a detailed description on the principle character of dentine micro-structure. Katz [6] and Hashin [7] analysed elastic properties of hard tissues, which focused on the constituent materials properties at the microscopic level, using bounding method including Vogit and Reuss as well as Hashin–Shtrikman. Kenney et al. [8] presented a critical review on mechanical properties of human dentine composites and indicated that the micro-structure of human dentine are hexagonal with the stiff direction perpendicular to the tubules, which is opposite to the predictions of the micro-mechanics. Most recently, Qin and Swain [2] extended the micro-mechanics models presented in [9–11] to the case of fully or partially saturated dentine composites by considering the actual detailed micro-structure of dentine composites [12–14]. However, the model (see Fig. 1) developed in [2] can provide analytical expressions for five effective material properties only (i.e., G_1^* shear modulus governing shear in any plane normal to the x_2x_3-plane; E_1^* longitudinal Young's modulus; E_2^* (or E_3^*) transverse Young's modulus in the plane perpendicular to the axial direction; K_{23}^* bulk modulus in the x_2x_3-plane; and v_{23}^* is the transverse Poisson's ratio in the same plane). As for the sixth effective constants, G_{23}^* shear modulus in the x_2x_3-plane, the model in [2] can only predict its upper and lower bounds. The limitation is attributable to the use of dilute model introduced by Hashin and Rosen [9]. To obtain analytical expression of G_{23}^* the Generalized Self Consistent Model in [15] which is referred to as the Three Phase Model (see Fig. 2) is extended to the case of dentine composites in this paper.

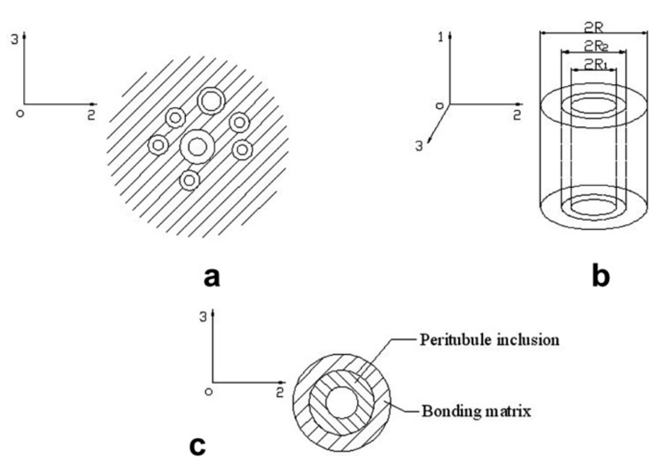

Fig. 1. Geometry of dentine composites and cell model [2]: (a) Cross-section of composite cylinder assemblage; (b) Unit cell model in axial direction; (c) Composite cylinders model.

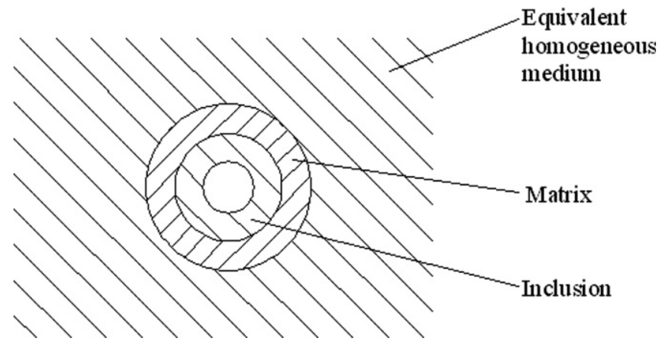

Fig. 2. Generalized self consistent model.

The proposed Generalized Self Consistent cell model is capable of modeling the dentine composites and the interaction among inclusions. In particular, it can provide closed-form expressions for all six effective material properties including G_{23}^*.

The derivation is based on the model presented in [2] and strain energy principle. Numerical results are presented to show the applicability of the proposed model and to study effect of Poisson's ratio and the volume fraction of inter-tubular dentine or peri-tubular dentine on material properties. Results obtained from the proposed theoretical model are compared with those from experimental observations presented in [1].

2. The unit cell model and basic equations

In this section, the micro-mechanics theory presented in [2] used to predict effective material properties of dentine composites is reviewed to establish notation and to provide a common source for reference in later sections. Concretely, at the micro-structural level, dentine is considered as a two-phase, fiber-reinforced composite material, one phase is the peri-tubular inclusion and the other is inter-tubular matrix (Fig. 1). Both of them are assumed to be isotropic and elastic. The peri-tubular dentine (inclusion phase in Fig. 1) is built up of collagen fibrils and mineralized hydroxyapatite, in which a porous phase (liquid or gas) is embedded in a connected solid phase forming the skeleton. The solid phase is linear elastic and isotropic. The porous phase is saturated with a fluid at the pressure p^{f}, or a gas at the pressure p^{g}. For a partially saturated porous media, Bishop suggested the following variation of Terzaghi's expression for the microscopic stress σ [10]

$$\sigma = C\varepsilon + \sigma^{\mathrm{fg}}, \tag{1}$$

with

$$C = \begin{cases} C_{\mathrm{s}} & \text{in } \Omega^{\mathrm{s}} \\ 0 & \text{otherwise} \end{cases}$$

$$\sigma^{\mathrm{fg}} = \begin{cases} 0 & \text{in } \Omega^{\mathrm{s}} \\ p^{\mathrm{c}} & \text{in } \Omega^{\mathrm{f}} \cup \Omega^{\mathrm{g}}, \end{cases} \tag{2}$$

where $p^{\mathrm{c}} = -p^{\mathrm{g}} + \zeta(p^{\mathrm{g}} - p^{\mathrm{f}})$, ε is microscopic strain, ζ is a parameter related to the degree of saturation and equals unity for fully saturate materials, C_s is the tensor of elastic moduli in the solid, Ω^s, Ω^f and Ω^g are domains occupied by the solid, fluid and gas phases, respectively. Their boundaries are denoted by $\partial\Omega^s$, $\partial\Omega^f$ and $\partial\Omega^g$.

It is known that the inclusion and matrix phases of dentine are themselves also three phases composites containing collagen fibrils, mineralized hydroxyapatite and liquid phase such as water or gas. The procedure for evaluating effective properties of peri-tubular inclusion and bonding matrix (i.e., Young's modules E_m, E_i and Poisson's ratios v_m, v_i where subscripts i and m refer to the isotropic inclusion and matrix, respectively) has been discussed in [2] (for more details see Sections 2 and 3 of [2]) and is omitted here.

The geometric model used in the analysis is shown in Fig. 2, a circular hollow cylindrical inclusion filled with liquid or gas phase is embedded in a concentric cylindrical annulus of the matrix material, which in turn is embedded in an infinite medium possessing the unknown effective properties. The effective material properties can be determined from the condition that the effective homogeneous medium possesses the same average values of stress and strain as does in the cylindrical model of Fig. 1. While, the effective homogeneous medium is transversely isotropic [3] and the stress–strain relation for a transversely isotropic porous material may be written in terms of six material constants in the form [2]:

$$\begin{Bmatrix} \sigma_{11} \\ \sigma_{22} \\ \sigma_{33} \\ \sigma_{12} \\ \sigma_{23} \\ \sigma_{31} \end{Bmatrix} = \begin{bmatrix} C_{11}^* & C_{12}^* & C_{12}^* & 0 & 0 & 0 \\ C_{12}^* & C_{22}^* & C_{23}^* & 0 & 0 & 0 \\ C_{12}^* & C_{23}^* & C_{22}^* & 0 & 0 & 0 \\ 0 & 0 & 0 & 2C_{44}^* & 0 & 0 \\ 0 & 0 & 0 & 0 & C_{22}^* - C_{23}^* & 0 \\ 0 & 0 & 0 & 0 & 0 & 2C_{44}^* \end{bmatrix} \times \begin{Bmatrix} \varepsilon_{11} \\ \varepsilon_{22} \\ \varepsilon_{33} \\ \varepsilon_{12} \\ \varepsilon_{23} \\ \varepsilon_{31} \end{Bmatrix} - q^* p^c \begin{Bmatrix} 1 \\ 1 \\ 1 \\ 0 \\ 0 \\ 0 \end{Bmatrix}. \tag{3}$$

where direction 1 is in the fiber direction and direction 2 and 3 are in the transverse plane. A convenient grouping of the six properties is given by [9]:

$$K_{23}^* = \frac{(C_{22}^* + C_{22}^*)}{2}, \tag{4}$$

$$G_{23}^* = \frac{(C_{22}^* - C_{23}^*)}{2}, \tag{5}$$

$$G_{12}^* = G_{13}^* = G_1^* = C_{44}^*, \tag{6}$$

$$E_1^* = C_{11}^* - \frac{2C_{12}^* C_{12}^*}{C_{22}^* + C_{23}^*}, \tag{7}$$

v_1^*, and q^*. Here G_{12}^* is a shear modulus governing shear in any plane normal to the transverse x_2x_3-plane; v_1^* is the Poisson's ratio for uniaxial stress in the x_1-direction, and q^* is the effective pore concentration coefficient. As was treated in Section 2 of [2], the superposition principle is used to decompose the load ($\mathbf{E}$, E_{ij} in the form of components, p^c) into two elementary loadings ($\mathbf{E}$, $p^c = 0$) and ($\mathbf{E} = 0$, p^c) [11]. For the loading case ($\mathbf{E} = 0$, p^c), the determination of q^* is similar to that in Section 2 of [2] and the final result which is consistent with that in [2]:

$$q^* = \frac{1}{2}\left(f_i q_i + (1 - f_i) q_m + \frac{q_i q_m}{f_i q_m + (1 - f_i) q_i}\right), \tag{8}$$

where f_i is the volume fraction of inclusion phase. Then for the loading case ($\mathbf{E}$, $p^c = 0$), the discussion is given as below.

3. Shear modulus G_{23}^*

To obtain analytical expression of G_{23}^*, a two-dimensional cell model is considered as shown in Fig. 2. It should be mentioned that the model shown in Fig. 2 is a hollow multi-layer cylinder, which is different from the solid cylinder used in [3,15]. Therefore, we need to re-derive all effective material constants for the hollow cylinder model. Since this is an axisymmetric problem a polar coordinate system is used with the origin at the center of the composite cylinder. As we can see from Fig. 2, there are three distinctive regions in which the solutions including the stresses and displacements must be obtained, respectively.

Following the way treated in [16], the stress functions $\varphi^{(1)}(z)$, $\phi^{(1)}(z)$, $\varphi^{(2)}(z)$ and $\phi^{(2)}(z)$ for the present problem can be obtained and are listed in Appendix A for the reader's convenience.

Using the solutions of equilibrium equation in [16] and the conditions of continuity for σ_r, $\tau_{r\theta}$, u_r and u_θ across the three interfaces between regions (Fig. 2), we have following 22 equations:

$\sigma_r^{(1)} - \mathrm{i}\tau_{r\theta}^{(1)} = 0$ stresses at $r = R_1$:

$$\left.\begin{aligned} &-a_{-1}^{(1)}\tfrac{R}{R_1^2} + \tfrac{a_3^{(1)}}{R^3} R_1^2 - b_{-3}^{(1)}\tfrac{R^3}{R_1^4} = 0, \\ &-3\tfrac{a_3^{(1)}}{R^3} R_1^2 - a_{-1}^{(1)}\tfrac{R}{R_1^2} + \tfrac{b_1^{(1)}}{R} = 0, \\ &\tfrac{a_2^{(1)}}{R^2} R_1 - b_{-2}^{(1)}\tfrac{R^2}{R_1^3} = 0, \\ &2\tfrac{a_1^{(1)}}{R} - b_{-1}^{(1)}\tfrac{R}{R_1^2} = 0. \end{aligned}\right\} \tag{9}$$

$\sigma_r^{(1)} - \mathrm{i}\tau_{r\theta}^{(1)} = \sigma_r^{(2)} - \mathrm{i}\tau_{r\theta}^{(2)}$ stresses at $r = R_2$:

$$\left.\begin{aligned} &-a_{-1}^{(1)}\tfrac{R}{R_2^2} + \tfrac{a_3^{(1)}}{R^3} R_2^2 - b_{-3}^{(1)}\tfrac{R^3}{R_2^4} = -a_{-1}^{(2)}\tfrac{R}{R_2^2} + \tfrac{a_3^{(2)}}{R^3} R_2^2 - b_{-3}^{(2)}\tfrac{R^3}{R_2^4}, \\ &-3\tfrac{a_3^{(1)}}{R^3} R_2^2 - a_{-1}^{(1)}\tfrac{R}{R_2^2} + \tfrac{b_1^{(1)}}{R} = -3\tfrac{a_3^{(2)}}{R^3} R_2^2 - a_{-1}^{(2)}\tfrac{R}{R_2^2} + \tfrac{b_1^{(2)}}{R}, \\ &\tfrac{a_2^{(1)}}{R^2} R_2 - b_{-2}^{(1)}\tfrac{R^2}{R_2^3} = \tfrac{a_2^{(2)}}{R^2} R_2 - b_{-2}^{(2)}\tfrac{R^2}{R_2^3}, \\ &2\tfrac{a_1^{(1)}}{R} - b_{-1}^{(1)}\tfrac{R}{R_2^2} = 2\tfrac{a_1^{(2)}}{R} - b_{-1}^{(2)}\tfrac{R}{R_2^2}. \end{aligned}\right\} \tag{10}$$

$\sigma_r^{(2)} - \mathrm{i}\tau_{r\theta}^{(2)} = \sigma_r - \mathrm{i}\tau_{r\theta}$ stresses at $r = R_3 = R$:

$$\left.\begin{aligned}&-a_{-1}^{(2)}+a_3^{(2)}-b_{-3}^{(2)}=-\alpha_{-1}-\beta_{-3},\\&-3a_3^{(2)}-a_{-1}^{(2)}+b_1^{(2)}=-\alpha_{-1}+2,\\&a_2^{(2)}-b_{-2}^{(2)}=-\beta_{-2},\\&2a_1^{(2)}-b_{-1}^{(2)}=2-\beta_{-1}.\end{aligned}\right\}\tag{11}$$

$u_r^{(1)}-\mathrm{i}u_\theta^{(1)}=u_r^{(2)}-\mathrm{i}u_\theta^{(2)}$ displacements at $r=R_2$:

$$\left.\begin{aligned}&G_\mathrm{m}\left(\chi_\mathrm{i}a_{-1}^{(1)}\tfrac{R}{R_2}-3a_3^{(1)}\tfrac{R_2^3}{R^3}+b_1^{(1)}\tfrac{R_2}{R}\right)=G_\mathrm{i}\left(\chi_\mathrm{m}a_{-1}^{(2)}\tfrac{R}{R_2}-3a_3^{(2)}\tfrac{R_2^3}{R^3}+b_1^{(2)}\tfrac{R_2}{R}\right),\\&G_\mathrm{m}\left(\chi_\mathrm{i}a_3^{(1)}\tfrac{R_2^3}{R^3}+a_{-1}^{(1)}\tfrac{R}{R_2}+b_{-3}^{(1)}\tfrac{R^3}{R_2^3}\right)=G_\mathrm{i}\left(\chi_\mathrm{m}a_3^{(2)}\tfrac{R_2^3}{R^3}+a_{-1}^{(2)}\tfrac{R}{R_2}+b_{-3}^{(2)}\tfrac{R^3}{R_2^3}\right),\\&G_\mathrm{m}\left(-2a_2^{(1)}\tfrac{R_2^2}{R^2}+b_0^{(1)}\right)=G_\mathrm{i}\left(-2a_2^{(2)}\tfrac{R_2^2}{R^2}+b_0^{(2)}\right),\\&G_\mathrm{m}\left(\chi_\mathrm{i}a_2^{(1)}\tfrac{R_2^2}{R^2}+b_{-2}^{(1)}\tfrac{R^2}{R_2^2}\right)=G_\mathrm{i}\left(\chi_\mathrm{m}a_2^{(2)}\tfrac{R_2^2}{R^2}+b_{-2}^{(2)}\tfrac{R^2}{R_2^2}\right),\\&G_\mathrm{m}\left(\chi_\mathrm{i}a_1^{(1)}\tfrac{R_2}{R}-a_1^{(1)}\tfrac{R_2}{R}+b_{-1}^{(1)}\tfrac{R}{R_2}\right)=G_\mathrm{i}\left(\chi_\mathrm{m}a_1^{(2)}\tfrac{R_2}{R}-a_1^{(2)}\tfrac{R_2}{R}+b_{-1}^{(2)}\tfrac{R}{R_2}\right).\end{aligned}\right\}\tag{12}$$

$u_r^{(2)}-\mathrm{i}u_\theta^{(2)}=u_r-\mathrm{i}u_\theta$ displacements at $r=R_3=R$:

$$\left.\begin{aligned}&G_\mathrm{m}(\chi\alpha_{-1}+2)=G_{23}^*(\chi_\mathrm{m}a_{-1}^{(2)}-3a_3^{(2)}+b_1^{(2)}),\\&G_\mathrm{m}(\alpha_{-1}+\beta_{-3})=G_{23}^*(\chi_\mathrm{m}a_3^{(2)}+a_{-1}^{(2)}+b_{-3}^{(2)}),\\&0=-2a_2^{(2)}+b_0^{(2)},\\&G_\mathrm{m}\beta_{-2}=G_{23}^*(\chi_\mathrm{m}a_2^{(2)}+b_{-2}^{(2)}),\\&G_\mathrm{m}(\chi-1+\beta_{-1})=G_{23}^*(\chi_\mathrm{m}a_1^{(2)}-a_1^{(2)}+b_{-1}^{(2)}),\end{aligned}\right\}\tag{13}$$

where $\chi_\mathrm{i}=3-4v_\mathrm{i}$, $\chi_\mathrm{m}=3-4v_\mathrm{m}$. However, there are 23 unknown constants including G_{23}^* to be determined. One more equation is required to fully determine the all 23 unknowns uniquely.

To determine the effective shear modulus G_{23}^*, we make use of the basic result obtained by Eshelby (Eq. (5.1) in [17]), namely, for a homogeneous medium containing an inclusion, the strain energy U, under applied displacement conditions, is determined by [15]:

$$U=U_0-\frac{1}{2}\int_S(T_\mathrm{i}^0u_\mathrm{ie}-T_\mathrm{ie}u_\mathrm{i}^0)\mathrm{d}s,\tag{14}$$

where S is the surface of the inclusion, U_0 is the strain energy in the same medium when it contains no inclusion, T_i^0 and u_i^0 are the tractions and displacements in the medium when it contains no inclusion and T_ie and u_ie are the corresponding quantities at the same point in the medium when it contains the inclusion. Our criterion for determining the effective properties requires the equality of strain energy in the heterogeneous media and in the equivalent homogeneous media. This condition can be written as

$$U_\mathrm{equiv}=U.\tag{15}$$

As mentioned above, the energy of the equivalent homogeneous medium, U_equiv, is clearly the same as the energy of the model shown in Fig. 2 if there is no inclusion. But from Eshelby's derivation and the corresponding definition of terms stated with (14), this energy is just given by U_0, the energy of the medium with no inclusion, and thus

$$U_\mathrm{equiv}=U_0.\tag{16}$$

Combing relations (15) and (16) with (14) gives the following energy statement to be satisfied:

$$\int_0^{2\pi}\left(\sigma_r^0u_{r\mathrm{e}}+\tau_{r\theta}^0u_{\theta\mathrm{e}}-\sigma_{r\mathrm{e}}u_r^0-\tau_{r\theta\mathrm{e}}u_\theta^0\right)_{r=R}\mathrm{d}\theta=0.\tag{17}$$

When the present problem having conditions of simple shear at infinity, it follows that

$$\left.\begin{aligned}&\sigma_r^0=\cos 2\theta, u_r^0=\tfrac{r}{2G_{23}^*}\cos 2\theta,\\&\sigma_{r\theta}^0=-\sin 2\theta, u_\theta^0=\tfrac{r}{2G_{23}^*}\sin 2\theta,\end{aligned}\right\}\tag{18}$$

and $u_{r\mathrm{e}}|_{r=R}$, $u_{\theta\mathrm{e}}|_{r=R}$, $\sigma_{r\mathrm{e}}|_{r=R}$ and $\sigma_{r\theta\mathrm{e}}|_{r=R}$ have already been obtained from the equation of equilibrium [16] and used in and (13). Thence carrying out the integration (17) gives the simple result:

$$\alpha_{-1}=0.\tag{19}$$

By now, there have been 23 independent equations and 23 unknown constants. These unknown constants can be thus determined uniquely from the 23 equations. After a lengthy process of algebraic reduction, the governing equation for G_{23}^* is found to be a quadratic equation:

$$A\left(\frac{G_{23}^*}{G_\mathrm{m}}\right)^2+B\left(\frac{G_{23}^*}{G_\mathrm{m}}\right)+D=0,\tag{20}$$

where A, $B$and D are listed in Appendix B.

It can be seen that Eq. (20) is identical to that in [3,15] when $\alpha=0$ (i.e., for a solid cylinder model).

4. Effective constants K_{23}^*, E_1^*, G_{12}^* and v_1^*

As mentioned in Section 3 above, the effective homogeneous medium possesses the same average values of stress and strain as those in the cylindrical model defined in Fig. 1 (Section 2 above). For example, if the cylindrical model in Fig. 1 is subjected to the remote boundary condition [9]:

$$u_i^0(S)=\varepsilon_{ij}^0x_j,\tag{21}$$

over its entire boundary surface S, we have $\bar{\varepsilon}_{ij}=\frac{1}{\Omega}\int_\Omega\varepsilon_{ij}\mathrm{d}\Omega=\bar{\varepsilon}_{ij}^*=\varepsilon_{ij}^0$ where u_i^0 and ε_{ij}^0 are displacement and strain components, respectively, x_j are surface coordinates, and n_j the components of the outward normal to S, Ω is the area (or volume in 3D model) of the cylindrical model in Fig. 1, and $\bar{\varepsilon}_{ij}^*$ is the average effective strain. This principle is used to derive theoretical expressions of the four effective constants mentioned above.

4.1. Plane strain bulk modulus K_{23}^*

Following the way in [9], the strain system associated with (21) is chosen to be:

$$\bar{\varepsilon}_{22}=\bar{\varepsilon}_{33}=\varepsilon,\tag{22}$$

and all the other strain components vanish. We have from (21) that

$$u_1 = 0; \quad u_2 = \varepsilon x_2; \quad u_3 = \varepsilon x_3 \quad r = R. \tag{23}$$

Thus, the boundary value problem (23) for the cylindrical model in Fig. 1 reduces to an elementary axially symmetric plane strain problem. The corresponding solution for radial displacement u_r and radial stress σ_{rr} can then be written in the form [18]:

$$u_r = Ar + \frac{B}{r}, \tag{24}$$

$$\sigma_{rr} = 2\overline{K}A - 2G\frac{B}{r^2}, \tag{25}$$

where $\overline{K}$ is the plane strain bulk modulus defined by $\overline{K} = \lambda + G$, λ is a Lamé modulus and G the shear modulus. A and B are arbitrary constants. The solutions (24) and (25) hold true for both inclusion region $R_1 \leqslant r \leqslant R_2$ and matrix region $R_2 \leqslant r \leqslant R$, if the related elastic moduli are used. While strains in the equivalent homogeneous media are $\bar{\varepsilon}^*_{22} = \bar{\varepsilon}^*_{33} = \varepsilon$ and $\bar{\varepsilon}^*_{11} = \bar{\varepsilon}^*_{12} = \bar{\varepsilon}^*_{13} = \bar{\varepsilon}^*_{23} = 0$. Consequently, we can obtain the stresses and displacements using the stress–strain relation (3) and the well-known linear strain–displacement relation. They are:

$$\left.\begin{aligned} &\sigma_{re} = 2\varepsilon K^*_{23}, \\ &u_{ze} = u_{\theta e} = 0, \quad u_{re} = \varepsilon r, \end{aligned}\right\} \tag{26}$$

where the subscript e refers to the equivalent homogeneous medium. There are five unknown constants in this problem which can be determined from following five boundary conditions:

$$\left.\begin{aligned} &\sigma_{ri} = 0, \ r = R_1, \\ &u_{ri} = u_{rm}, \quad \sigma_{ri} = \sigma_{rm}, \quad r = R_2, \\ &u_{rm} = u_{re}, \quad \sigma_{rm} = \sigma_{re}, \quad r = R. \end{aligned}\right\} \tag{27}$$

Solving Eq. (27) we have

$$K^*_{23} = \overline{K}_m \frac{\phi(1-\alpha^2)(1+2\nu_m f_t) + 2\nu_m f_m\left(1+\frac{\alpha^2}{2\nu_i}\right)}{\phi(1-\alpha^2)f_m + (f_t + 2\nu_m)\left(1+\frac{\alpha^2}{2\nu_i}\right)}, \tag{28}$$

where $\phi = \frac{\overline{K}_i}{\overline{K}_m}$, $\alpha = \frac{R_1}{R_2}$, $f_t = \frac{R_2^2}{R^2}$, $f_m = 1 - f_t$, $\overline{K}_\gamma = \lambda_\gamma + G_\gamma (\gamma = \mathrm{i}, \mathrm{m})$.

4.2. Longitudinal Young's modulus E^*_1 and Poisson's ratio ν^*_1

The effective longitudinal Young's modulus E^*_1 can be determined by setting [19]:

$$\bar{\varepsilon}_{11} = \varepsilon, \quad \bar{\sigma}_{22} = \bar{\sigma}_{33} = \bar{\sigma}_{12} = \bar{\sigma}_{23} = \bar{\sigma}_{31} = 0. \tag{29}$$

The loading case (29) induces following displacement solution:

$$\left.\begin{aligned} &u_{ri} = A_i r + \tfrac{B_i}{r}, \quad R_1 \leqslant r \leqslant R_2, \\ &u_{rm} = A_m r + \tfrac{B_m}{r}, \quad R_2 \leqslant r \leqslant R, \\ &u_{re} = A_e r, \quad A_e = -\nu^*_1 \varepsilon, \\ &u_{\theta e} = 0, \\ &u_z = \varepsilon z, \quad r \geqslant R_1. \end{aligned}\right\} \tag{30}$$

The five unknown constants in (30) are determined using the following five boundary conditions:

$$\left.\begin{aligned} &\sigma_{ri} = 0, \ r = R_1, \\ &u_{ri} = u_{rm}, \ \sigma_{ri} = \sigma_{rm}, \ r = R_2, \\ &u_{rm} = u_{re}, \ \sigma_{rm} = \sigma_{re}, \ r = R. \end{aligned}\right\} \tag{31}$$

In the context of the present problem, the effective modulus E^*_1 is defined by [19]:

$$E^*_1 = \frac{1}{\pi b^2 \varepsilon} \int\int_\Omega \sigma_z(r) \mathrm{d}\Omega, \tag{32}$$

where Ω is the cross-section area of the cylindrical model in Fig. 1. In the end, the substitution of the solutions (31) into (32) and carrying out the integration (32) gives:

$$E^*_1 = E_m\left(f_i \frac{E_i}{E_m} + f_m\right)\frac{E_m(D_1 - D_3F_1) + E_i(D_2 - D_4F_2)}{E_m(D_1 - D_3) + E_i(D_2 - D_4)}, \tag{33}$$

where

$$\left.\begin{aligned} &D_1 = \tfrac{1+\alpha^2}{1-\alpha^2} - \nu_i, \quad D_2 = \tfrac{1+f_t}{f_m} + \nu_m, \\ &D_3 = \tfrac{2\nu_i^2}{1-\alpha^2}, \quad D_4 = 2\nu_m^2 \tfrac{f_t}{f_m}, \\ &F_1 = \tfrac{\nu_m f_i E_i + \nu_i f_m E_m}{\nu_i f_i E_i + f_m E_m}, \quad F_2 = \tfrac{\nu_i}{\nu_m} F_1. \end{aligned}\right\} \tag{34}$$

The effective Poisson's ratio ν^*_1 is determined by using the definition [19]:

$$\nu^*_1 = -\frac{u_r|_{r=R}}{\varepsilon R}. \tag{35}$$

Substituting Eqs. (30) and (31) into (35) we have

$$\nu^*_1 = \frac{f_i E_i L_1 + f_m E_m L_2 \nu_m}{f_i E_i L_3 + f_m E_m L_2}, \tag{36}$$

where

$$\left.\begin{aligned} &L_1 = 2\nu_i(1-\nu_m^2)f_t + f_m(1+\nu_m)\nu_m, \\ &L_2 = f_t\left[(1+\nu_m)\alpha^2 + 1 - \nu_i - 2\nu_i^2\right], \\ &L_3 = 2(1-\nu_m^2)f_t + (1+\nu_m)f_m. \end{aligned}\right\} \tag{37}$$

4.3. Shear modulus G^*_{12}

To obtain the solution of Shear modulus G^*_{12}, consider the following strain system [9]:

$$\bar{\varepsilon}_{12} = \bar{\varepsilon}_{21} = \frac{\gamma}{2}, \quad \bar{\varepsilon}_{11} = \bar{\varepsilon}_{22} = \bar{\varepsilon}_{33} = \bar{\varepsilon}_{13} = \bar{\varepsilon}_{23} = 0. \tag{38}$$

The displacement components induced by loading condition (38) are:

$$\left.\begin{aligned} &u_{ri} = C_i z\cos\theta, \quad u_{rm} = C_m z\cos\theta, \\ &u_{\theta i} = -C_i z\sin\theta, \quad u_{\theta m} = -C_m z\sin\theta, \\ &u_{zi} = \left(A_i r + \tfrac{B_i}{r}\right)\cos\theta, \quad u_{zm} = \left(A_m r + \tfrac{B_m}{r}\right)\cos\theta, \\ &u_{re} = \gamma z\cos\theta, \quad u_{\theta e} = -\gamma z\sin\theta, \\ &u_{ze} = 0. \end{aligned}\right\} \tag{39}$$

The eight unknowns in (39) are determined by the following boundary and continuity conditions:

$$\left.\begin{array}{l}\sigma_{rzi}=0, \quad r=R_1,\\ \sigma_{rzi}=\sigma_{rzm}, \quad u_{ri}=u_{rm}, \quad u_{\theta i}=u_{\theta m}, \quad r=R_2,\\ \sigma_{rzm}=\sigma_{rze}, \quad u_{rm}=u_{re}, \quad u_{\theta m}=u_{\theta e}, u_{zm}=u_{ze}, \quad r=R.\end{array}\right\} \tag{40}$$

Finally, we derive the shear modulus:

$$G_1^*=G_m\frac{\eta(1-\alpha^2)(1+f_t)+f_m(1+\alpha^2)}{\eta(1-\alpha^2)f_m+(1+\alpha^2)(1+f_t)}, \tag{41}$$

where $\eta=\frac{G_i}{G_m}, \alpha=\frac{R_1}{R_2}, f_t=\frac{R_2^2}{R^2}, f_m=1-f_t$.

It is interesting to note that the resulting expressions of effective material constants, except G_{23}^*, is exactly the same as those obtained in [2], where different cell model has been used.

5. Numerical results and discussion

Since the five properties K_{23}^*, E_1^*, G_1^*, v_1^* and q^* obtained above are the same as those presented in [2], we need only to present the numerical results for G_{23}^* and the others can refer to [2] for detailed numerical results. In order to allow for comparisons with Kinney's results [1], the elastic properties of the peri-tubule inclusion and bonding matrix which have been analysed by nano-indentation method [1,20] are assumed:

$$E_i=22.5\ \text{GPa}, \quad v_i=0.25, \quad E_m=15\ \text{GPa}, \quad v_m=0.1. \tag{42}$$

By checking the data given in [21,22], it is noted that $\alpha=\frac{R_1}{R_2}$ is independent of position although both R_1 and R_2 vary from the pulp to the dentine–enamel junction. The results of G_{23}^* from the proposed model are listed in Table 1 and compared with those presented in [1].

From the table above we can see that the present results are in good agreement with those presented in [1]. Further, making use of (20), the magnitudes of the transverse shear modulus G_{23}^* (GPa) are charted in Figs. 3 and 4, respectively, as a function of the volume fraction of inter-tubular f_m and peri-tubular dentine f_i with different values of v_m (=0.1, 0.25, 0.4). As was expected, the modulus G_{23}^* decreases linearly with the volume fraction of inter-tubular dentine and increases linearly with the volume fraction of peri-tubular dentine. This conclusion is consistent with that reported from [1]. It is also observed that G_{23}^* decreases with the Poisson's ratio of inter-tubular matrix at the same volume fraction of the matrix or inclusion phase.

Table 1
The elastic modulus of G_{23}^* (GPa) at some typical points and comparison is made with those predicted by [1]

Tubular concentration	Present results	Results in [1]
0.05	6.88	6.90
0.10	6.94	6.99
0.15	7.00	7.09
0.20	7.07	7.11
0.25	7.13	7.20

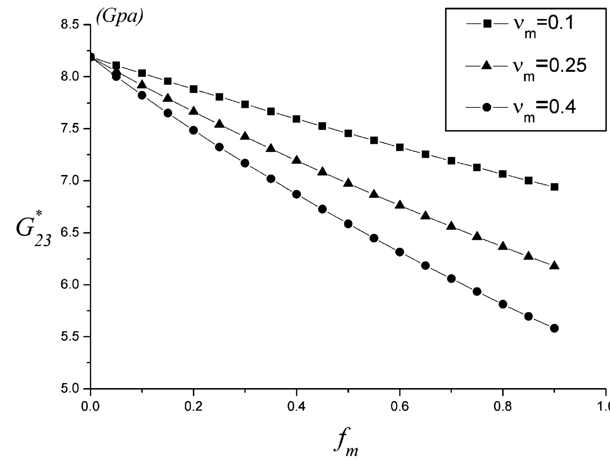

Fig. 3. Transverse shear modulus as a function of the volume fraction of inter-tubular dentine for three values of the Poisson's ratio of the matrix.

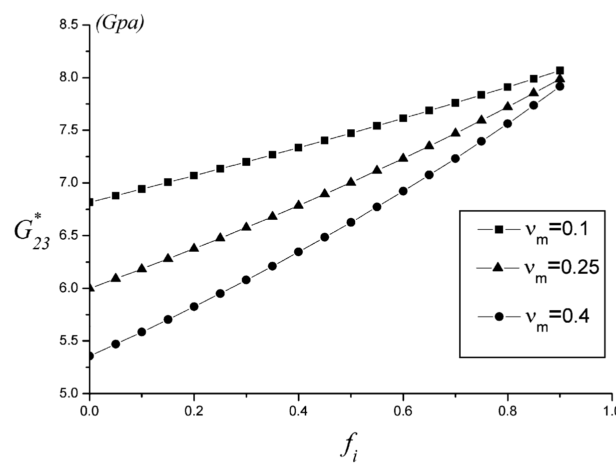

Fig. 4. Transverse shear modulus as a function of the volume fraction of peri-tubular dentine for three values of the Poisson's ratio of the matrix.

6. Conclusions

In this paper, taking the actual structure of dentine into consideration and considering the interaction among inclusions, we have developed a Generalized Self Consistent Model for predicting the effective material properties of dentine composites. The model consists of a circular hollow cylindrical inclusion filled with liquid or gas phase is embedded in a concentric cylindrical annulus of the matrix material, which in turn is embedded in an infinite medium possessing the unknown effective properties we need to obtain. Further, each layer of the cylindrical shells called the inclusion and matrix phase is here considered as a composite consisting of collagen fibrils, with mineralized hydroxyapatite, and water (or gas in the case of dry dentine composites). Importantly, an analytical solution for the transverse shear modulus G_{23}^* is obtained and can be reduced to the solid cylinder model in [3,15] when $\alpha=0$. A numerical comparison is made between the proposed results and the prediction obtained in [1] and a good agreement between them is observed. Obviously, the theoretical expression for G_{23}^{*} is more economical and acceptable to predict the effective properties of dentine compared with conventional biomechanical testing methods in engineering activities.

Acknowledgement

This work was financially supported by the Australian Research Council. The supports are fully acknowledged.

Appendix A. Stress functions of the present problem

$$\left.\begin{aligned}\varphi^{(1)}(z) &= \frac{R}{2}\sum_{k=-1}^{3} a_k^{(1)}\frac{z^k}{R^k},\\ \phi^{(1)}(z) &= -\frac{R}{2}\sum_{k=-3}^{1} b_k^{(1)}\frac{z^k}{R^k},\end{aligned}\right\} R_1 \leqslant r \leqslant R_2.$$

$$\left.\begin{aligned}\varphi^{(2)}(z) &= \frac{R}{2}\sum_{k=-1}^{3} a_k^{(2)}\frac{z^k}{R^k},\\ \phi^{(2)}(z) &= -\frac{R}{2}\sum_{k=-3}^{1} b_k^{(2)}\frac{z^k}{R^k},\end{aligned}\right\} R_2 \leqslant r \leqslant R.$$

$$\left.\begin{aligned}\varphi(z) &= \frac{R}{2}\left[\sum_{k=1}^{1} A_k\frac{z^k}{R^k} + \sum_{k=1}^{1}\alpha_{-k}\frac{R^k}{z^k}\right],\\ \phi(z) &= -\frac{R}{2}\left[\sum_{k=0}^{1} B_k\frac{z^k}{R^k} + \sum_{k=1}^{3}\beta_{-k}\frac{R^k}{z^k}\right],\end{aligned}\right\} r \geqslant R.$$

While the stress vector $\sigma_r - i\tau_{r\theta}$ and the displacement vector $u_r - \mathrm{i}u_\theta$ can be expressed by means of the stress functions $\varphi(z)$ and $\phi(z)$ as

$$\left.\begin{aligned}\sigma_r - \mathrm{i}\tau_{r\theta} &= \varphi'(z) + \overline{\varphi}''(z) - \mathrm{e}^{2i\theta}[\bar{z}\varphi''(z) + \phi'(z)],\\ u_r - \mathrm{i}u_\theta &= \frac{1}{2G}[\chi\overline{\varphi}(z) - \bar{z}\varphi'(z) - \phi(z)]\mathrm{e}^{\mathrm{i}\theta},\end{aligned}\right\}$$

where G is shear modulus and $\chi = 3 - 4v$, v is the Poisson's ratio.

Appendix B. The parameters A, B, and D in (20)

$$\begin{aligned}A = {} & \{[L\eta^2 + [(\alpha^8 - \alpha^2)\chi_\mathrm{i} + (\alpha^2 - 1)(4\alpha^4 - 2\alpha^2 + 1)]\eta]\chi_\mathrm{m}^2\\ & + (O + M + L\eta^2)\chi_\mathrm{m}\}f_\mathrm{t}^4 + Tf_\mathrm{t}^3 + 6Sf_\mathrm{t}^2\\ & + [(Q + M - 18\alpha^4 - 6)\chi_\mathrm{m}^2 + 3Q + 3M]f_\mathrm{t}\\ & + (L\eta^2 - O)\chi_\mathrm{m}^2 + \{[(-\alpha^8 + \alpha^2)\chi_\mathrm{i} + L - \alpha^8 + \alpha^2]\eta\\ & + \chi_\mathrm{i}^2\alpha^2 + 4\alpha^6 - 6\alpha^4 + 3\alpha^2\}\chi_\mathrm{m},\end{aligned}$$

$$\begin{aligned}B = {} & \{[[(\alpha^8 - 2\alpha^2 + 1)\chi_\mathrm{i} + 8\alpha^6 - 12\alpha^4 + 6\alpha^2 - 1]\eta - M]\chi_\mathrm{m}\\ & + O + M + L\eta^2 + (-L\eta^2 - N)\chi_\mathrm{m}^2 f_\mathrm{t}^4 - 2Tf_\mathrm{t}^3 - 12Sf_\mathrm{t}^2\\ & + 2(-Q - M)(3 - \chi_\mathrm{m})f_\mathrm{t} + (O - L\eta^2)\chi_\mathrm{m}^2 + (-Q - M)\chi_\mathrm{m}\\ & + [(-\alpha^8 + \alpha^2)\chi_\mathrm{i} - 4\alpha^6 + 6\alpha^4 - 3\alpha^2 + 1]\eta + M + L\eta^2\end{aligned}$$

$$\begin{aligned}D = {} & \{(-N - L\eta^2)\chi_\mathrm{m} - O - M - L\eta^2\}f_\mathrm{t}^4 + Tf_\mathrm{t}^3\\ & + 6\{[(-\alpha^4 + \alpha^2)\chi_\mathrm{i} - \alpha^4 + \alpha^2]\eta\chi_\mathrm{m} + [(\alpha^8 - \alpha^4 - \alpha^2 + 1)\chi_\mathrm{i}\\ & - \alpha^8 + 8\alpha^6 - 13\alpha^4 + 7\alpha^2 - 1]\eta - M\}f_\mathrm{t}^2 + 4(Q + M)f_\mathrm{t}\\ & + (O - L\eta^2)\chi_\mathrm{m} + N - M - L\eta^2,\end{aligned}$$

where

$$\eta = \frac{G_\mathrm{i}}{G_\mathrm{m}}, \alpha = \frac{R_1}{R_2}, f_\mathrm{t} = \frac{R_2^2}{R^2}$$

$$O = [(\alpha^2 - 1)\chi_\mathrm{i} + L + \alpha^2 - 1]\eta$$

$$N = [(\alpha^8 - \alpha^2)\chi_\mathrm{i} + 4\alpha^6 - 6\alpha^4 + 3\alpha^2 - 1]\eta$$

$$L = \alpha^8 - 4\alpha^6 + 6\alpha^4 - 4\alpha^2 + 1 = (a^2 - 1)^4$$

$$M = \chi_\mathrm{i}^2\alpha^2 + (\alpha^8 + 1)\chi_\mathrm{i} + (4\alpha^6 - 6\alpha^4 + 3\alpha^2 - L\eta^2)$$

$$Q = [(-\alpha^8 + 2\alpha^2 - 1)\chi_\mathrm{i} + \alpha^8 - 8\alpha^6 + 12\alpha^4 - 6\alpha^2 + 1]\eta$$

$$\begin{aligned}T = {} & [(\alpha^8 + 6\alpha^4 - 8\alpha^2 + 1)\chi_\mathrm{i} - \alpha^8 + 8\alpha^6 - 6\alpha^4 - 1]\eta\chi_\mathrm{m}\\ & + 4M + L\eta^2 + 3[-(\alpha^4 - 1)^2\chi_\mathrm{i} + \alpha^8 - 8\alpha^6 + 14\alpha^4\\ & - 8\alpha^2 + 1]\eta - L\eta^2\chi_\mathrm{m}^2\end{aligned}$$

$$\begin{aligned}S = {} & [(\alpha^8 - \alpha^4 - \alpha^2 1)\chi_\mathrm{i} - \alpha^8 + 8\alpha^6 - 13\alpha^4 + 7\alpha^2 - 1]\eta\\ & + (-\alpha^4 + \alpha^)(\chi_\mathrm{i} + 1)\eta\chi_\mathrm{m} - M\end{aligned}$$

References

[1] Kinney JH, Balooch M, Marshall GW, Marshall SJ. A micromechanics model of the elastic properties of human dentine. Arch Oral Biol 1999;44:813–22.
[2] Qin QH, Swain MV. A micro-mechanics model of dentin mechanical properties. Biomaterials 2004;25:5081–90.
[3] Christensen RM. A critical evaluation for a class of micro-mechanics models. J Mech Phys Solids 1990;38:379–404.
[4] Currey JD. The effect of porosity and mineral content on the young's modulus of elasticity of compact bone. J Biomech 1988;21:131–9.
[5] Jones SJ, Boyde A. Ultrastructure of dentin and dentinogenesis. In: Linde A, editor. Dentin and dentinogenesis. Boca Raton: CRC Press; 1984. p. 81–134.
[6] Katz JL. Hard tissue as a composite material—I. Bounds on the elastic behaviour. J Biomech 1971;4:455–73.
[7] Hashin Z. Analysis of composite materials—A survey. J Appl Mech 1983;50:481–503.
[8] Kinney JH, Marshall SJ, Marshall GW. The mechanical properties of human dentin: A critical review and re-evaluation of the dental literature. Crit Rev Oral Biol Med 2003;14:13–29.
[9] Hashin Z, Rosen BW. The elastic moduli of fiber reinforced materials. J Appl Mech 1964;31:223–32.
[10] Skempton WW. Effective stress in soils. In: Conference Organized by the British National Society of Foundations Engineer at ICE, March 30–31. London: Butterworth; 1962. p. 4–16.
[11] Dormieux L, Molinari A, Knodo D. Micromechanical approach to the behavior of poroelastic materials. J Mech Phys Solids 2002;50:2031–203.
[12] Marshall GW, Marshall SJ, Kinney JH, Balooch M. The dentin substrate: Structure and properties related to bonding. J Dent 1997;25:441–58.
[13] Marshall GW, Balooch M, Gallagher RR, Gansky SA, Marshall SJ. Mechanical properties of the dentinoenamel junction: AFM studies of nanohardness, elastic modulus, and fracture. J Biomed Mater Res 2001;54:87–95.
[14] Xu HHk, Smith DT, Jahanmir S, Romberg E, Kelly JR, Thompson VP, et al. Indentation damage and mechanical properties of human enamel and dentin. J Dent Res 1998;77:472–80.
[15] Christensen RM, Lo KH. Solutions for effective shear properties in three phase sphere and cylinder models. J Mech Phys Solids 1979;27:315–30.
[16] Savin GN. Stress Concentration Around Holes. Oxford: Pergamon Press; 1961. pp. 234–244.

[17] Eshelby JD. The continuum theory of lattice defects. In: Seitz F, Turnbull D, editors. Progress in Solid State Physics, Vol. 3. New York: Academic; 1956. p. 79.
[18] Love AEH. A treatise on the mathematical theory of elasticity. New York, NY: Dover Publications, Inc; 1944.
[19] Christensen RM. Mechanics of Composite Materials. New York: Wiley-International Publication. John Wiley and Sons; 1979. p. 81.
[20] Marshall GW, Habelitz S, Gallagher R, Balooch M, Balooch G, Marshall SJ. Nanomechanical properties of hydrated carious human dentine. J Dent Res 2001;80:1768–71.
[21] Palshley DH. Dentin: a dynamic substrate – A review. Scan Microsc 1989;3:161–76.
[22] Garberoglio R, Brannstrom M. Scanning electron Microscopy investigation of human dentinal tubules. Arch Oral Biol 1976;21:355–62.